Journal of Solid State Chemistry 183 (2010) 1490–1495

Contents lists available at ScienceDirect

Journal of Solid State Chemistry

journal homepage: www.elsevier.com/locate/jssc

The effects of high magnetic field on the morphology and microwave electromagnetic properties of MnO_2 powder

Jia Zhang [a], Duan Yuping [a,*], Li Shuqing [b,1], Li Xiaogang [c,2], Liu Shunhua [a]

[a] Department of Materials Processing Engineering, School of Materials Science & Engineering, Dalian University of Technology, Linggong Road 2, Ganjingzi District, Dalian 116085, Liaoning Province, PR China

[b] Beijing Aeronautical Manufacturing Technology Research Institute, 1 Jun Zhuang east Road, Chaoyang District, Beijing 100024, PR China

[c] School of Materials Science and Engineering, University of Science and Technology Beijing, 30 Xueyuan Road, Haidian District, Beijing 100083, PR China

ARTICLE INFO

Article history:
Received 11 December 2009
Received in revised form
14 April 2010
Accepted 17 April 2010
Available online 28 April 2010

Keywords:
Manganese dioxides
High magnetic field
Chain shape
Electromagnetic properties

ABSTRACT

MnO_2 with a sea urchin-like ball chain shape was first synthesized in a high magnetic field via a simple chemical process, and a mechanism for the formation of this grain shape was discussed. The as-synthesized samples were characterized by XRD, SEM, TEM, and vector network analysis. The dielectric constant and the loss tangent clearly decreased under a magnetic field. The magnetic loss tangent and the imaginary part of the magnetic permeability increased substantially. Furthermore, the theoretically calculated values of reflection loss showed that the absorption peaks shifted to a higher frequency with increases in the magnetic field strength.

1. Introduction

Shape- and size-controlled dispersible inorganic nanocrystals such as metals, semiconductors, and metal oxides, have been the subject of intensive research because of their potential applications in electronics, photonics, and catalysis [1,2]. They are also ideal subjects for research on optical, electrical, magnetic, microwave electromagnetic, mechanical properties, and the interdependence of these characteristics on morphology and size confinement [3–5]. Consequently, particles with novel shapes and sizes have become especially interesting.

In this context, manganese dioxides and their derivative compounds have attracted special attention. Their outstanding structural flexibility, in combination with their novel chemical and physical properties has paved the way for their wide use as catalysts [6], molecular sieves [7], and Li/MnO_2 batteries materials [8]. The different crystallographic structural forms of MnO_2 that exist in nature, such as the α-, β-, γ-, δ-, and other types [9], are generally believed to be responsible for their unique properties. For example, Bach et al. have pointed out that the electrochemical properties of MnO_2 are strongly dependent on parameters such as powder morphology, crystalline structure, or bulk density [10].

Several research groups have investigated the MnO_2 with different crystalline structures. They have successfully prepared nanorods [1,11–13], nanofibers [14,15], cuneiforms [2], microspheres [16], and nanowires [17] of α-MnO_2, β-MnO_2, γ-MnO_2, and δ-MnO_2. Manganese oxide resembling a "sand rose" with large blades was synthesized by Beaudrouet [18]. Nest-like hierarchical architecture of manganese oxide was studied by Liu et al. [19]. Cheng et al. [20] synthesized a 2-D hexagonal star-like β-MnO_2. Zhang et al. [21] obtained hollow octahedral of manganese oxides. However, most of these studies used the method of hydrothermal synthesis to obtain manganese oxides without any external field, and there are only a few research papers on the hydrothermal synthesis under the high magnetic field. One of these is by Zhong and the co-author [22], which focused only on the electrochemistry property of the prepared MnO_2 powder. The microwave electromagnetic characteristics of the prepared MnO_2 under the high magnetic field were not dealt with.

Many researchers have synthesized other materials in high magnetic field and obtained good morphology. Gong et al. [23] were able to fabricate Ni fibers of different lengths by applying external magnetic fields. Polyaniline with an open-ramified rod-like pattern was obtained under the high magnetic field by Duan [5]. External magnetic fields can therefore be viewed as important components of synthetic processes for generation of unusually shaped materials.

In the present paper, manganese oxide with the sea urchin-like ball chain shape was first synthesized in a high magnetic field, and the microwave electromagnetic characteristics of the

* Corresponding author. Fax: +86 411 84709284.
E-mail addresses: duanyp@dlut.edu.cn (D. Yuping), lsq6668@126.com (L. Shuqing), lixiaogang99@263.net (L. Xiaogang).
[1] Fax: +86 10 85701102.
[2] Fax: +86 10 62327878.

0022-4596/$ - see front matter © 2010 Elsevier Inc. All rights reserved.
doi:10.1016/j.jssc.2010.04.027

prepared MnO_2 were also studied firstly. Moreover, a mechanism for formation of the observed grain shape by a high magnetic field was discussed.

2. Experimental

All chemical reagents were commercially available and were used as-received without further purification. Manganese sulfate ($MnSO_4 \cdot H_2O$) and ammonium persulfate ($(NH_4)_2S_2O_8$) were purchased from the Dalian Shenlian Chemical Reagent, Co. (China). The procedures of a typical synthesis are described below.

2.1. Synthesis

A solution of $MnSO_4$ was prepared by dissolving 5.1 g in 100 mL distilled water. The obtained solution was stirred until the solution was transparent, then 17.1 g $(NH_4)_2S_2O_8$ was added and stirring was continued for another 30 min at room temperature. The transparent solution was then transferred to a glass test tube and heated at 70 °C for 4 h in a high magnetic field, at selected magnetic field strengths of 1, 3, 5 or 8 T. Subsequently, the glass test tube was allowed to cool to room temperature. The black products were filtered off, washed several times with distilled water and absolute ethanol, and then dried under vacuum at 60 °C for 24 h. The product, a black powder, was collected for characterization.

2.2. Characterization

Phase identifications were performed by the X-ray powder diffraction (SHIMADZU, XRD-6000, 40 kV/30 mA) with Cu$K\alpha$ radiation ($\lambda = 0.15406$ nm) in the 2θ range of 10° to 100° in steps of 0.04°, using the detector technique for measuring intensities. Microstructural features of the MnO_2 were observed by electron microscopy (SEM, JSM-5600LV). Transmission electron microscope (TEM) images, high resolution TEM (HRTEM) images, and selected area electron diffraction (SAED) patterns were generated using a TECNAI $G^2$20 S-Twin TEM.

The measurements of complex relative permittivity and permeability versus frequency were carried out by reflection/transmission technology using an Agilent 8722ES network analyzer. The as-obtained MnO_2 was dispersed in molten paraffin wax, and the uniform mixtures were molded into toroid-shaped samples of 7.00 mm outer diameter and 3.00 inner diameter. The specimens, consisting of 30 wt% MnO_2 powders, were measured at 2–18 GHz. The microwave absorption properties of the MnO_2/paraffin wax samples were calculated according to the transmit line theory.

3. Results and discussion

3.1. Morphology analysis

A series of experiments were carried out by varying the magnetic field strength, and the morphologies of the resulting MnO_2 products obtained were examined by SEM and TEM. Figs. 1 and 2 show the SEM and TEM images with inserted diffraction patterns and the HRTEM images prepared in the present study. The five samples corresponding to Fig. 1 and Fig. 2 (a–e) were obtained at 70 °C for 4 h with the magnetic field strengths of 0, 1, 3, 5, and 8 T, respectively. As can be seen in Fig. 1 and 2 (a), sea urchin-like microspheres can be observed in the precipitated sample. At the magnetic field strength of 1 T, the microspheres began to form sea urchin-like ball chain structures (Fig. 1 and 2 (b)), but this was not very pronounced. With magnetic field strengths of 3 to 8 T, the sea urchin-like ball chain pattern became more evident (Figs. 1 and 2 (c–e)). From Fig. 1, the effect of high magnetic field on the microspheres size was only slightly, but it is obvious from Fig. 2 that the particle size of the sample 3 T is smaller and more uniform than others. The inserted diffraction pattern images in Fig. 2 show that the crystallization degree of the MnO_2 in a high magnetic field was improved effectively compared with that without high magnetic field. And the HRTEM images provide more detailed structural information about the stick on the surface of the micro-sphere, showing the apparent lattice fringes of the crystal. But the influence of the high magnetic field on lattice fringes of the crystal is not very evident.

One possible mechanism for the formation of the sea urchin-like ball chain shape is the following. The original sea urchin-like microspheres were arrayed randomly in the absence of a high magnetic field. Nevertheless, the microspheres arrayed themselves along a given direction under the external magnetic field (Fig. 1 (c–e)). This is because, for any kind of crystals, differences in the arrangement and the density of the atomic structure will result in differences in the magnetic susceptibilities of the same crystal at different crystallographic orientations. Small size microspheres arrayed along the direction of their maximum magnetic susceptibility (which is also along the magnetic field) were equivalent to small magnetic bodies. Consequently, they assembled to form the sea urchin-like ball chain shaped.

3.2. Phase structure and compositional analysis

According to Fig. 3, the α-MnO_2 and γ-MnO_2 are the major MnO_2 products, and all of the diffraction peaks can be indexed to tetragonal and orthorhombic structures (PDF# 721982, PDF# 822169, PDF# 721983 and PDF# 731539). The broadened diffraction peaks indicate that the crystalline size of the samples is small and that the crystallinity is not yet ideal. Further more, it is obvious that the crystalline nature and percentage of α- and γ-phase MnO_2 in each sample are different from the X-ray results, which show that the high magnetic field has a significant effect on the crystalline nature and the phase structure.

3.3. Electromagnetic properties

The complex permittivity, permeability, and their loss tangent represent the dielectric and magnetic properties of an absorbing material. The real parts (ε' and μ') of complex permittivity and permeability symbolize the storage capability of electric and magnetic energy. The imaginary parts (ε'' and μ'') represent the loss of electric and magnetic energy [24]. The loss tangent ($tg\delta$) represents the loss properties of incidence electromagnetic wave in the microwave absorber. In terms of microwave absorption, the imaginary parts and the loss tangent are expected to be larger.

Fig. 4 shows the relatively complex permittivity and permeability of the five samples in the frequency range 2–18 GHz. As shown in Fig. 4 (a), the ε' values for the five samples declined from 9.29, 9.39, 7.77, 4.64 and 5.06 to 5.26, 5.29, 5.03, 3.38 and 3.72, respectively, with increasing frequency in the 2–18 GHz range. All of the ε'' values for the five samples also exhibited a decrease from 3.43, 3.72, 2.54, 0.93 and 1.04 to 2.20, 2.27, 1.64, 0.75 and 0.83, respectively, as frequency was increased from 2 to 18 GHz. Increases in magnetic field strength from 0 to 8 T resulted in decreases in ε' values of the samples, except for 8 T and ε'' values, decreased. Fig. 4 (b) shows that the μ' and μ'' values of samples, except for 3 and 5 T, were almost constant, with less variation throughout the whole frequency range. All $\mu' \approx 1.04$ and

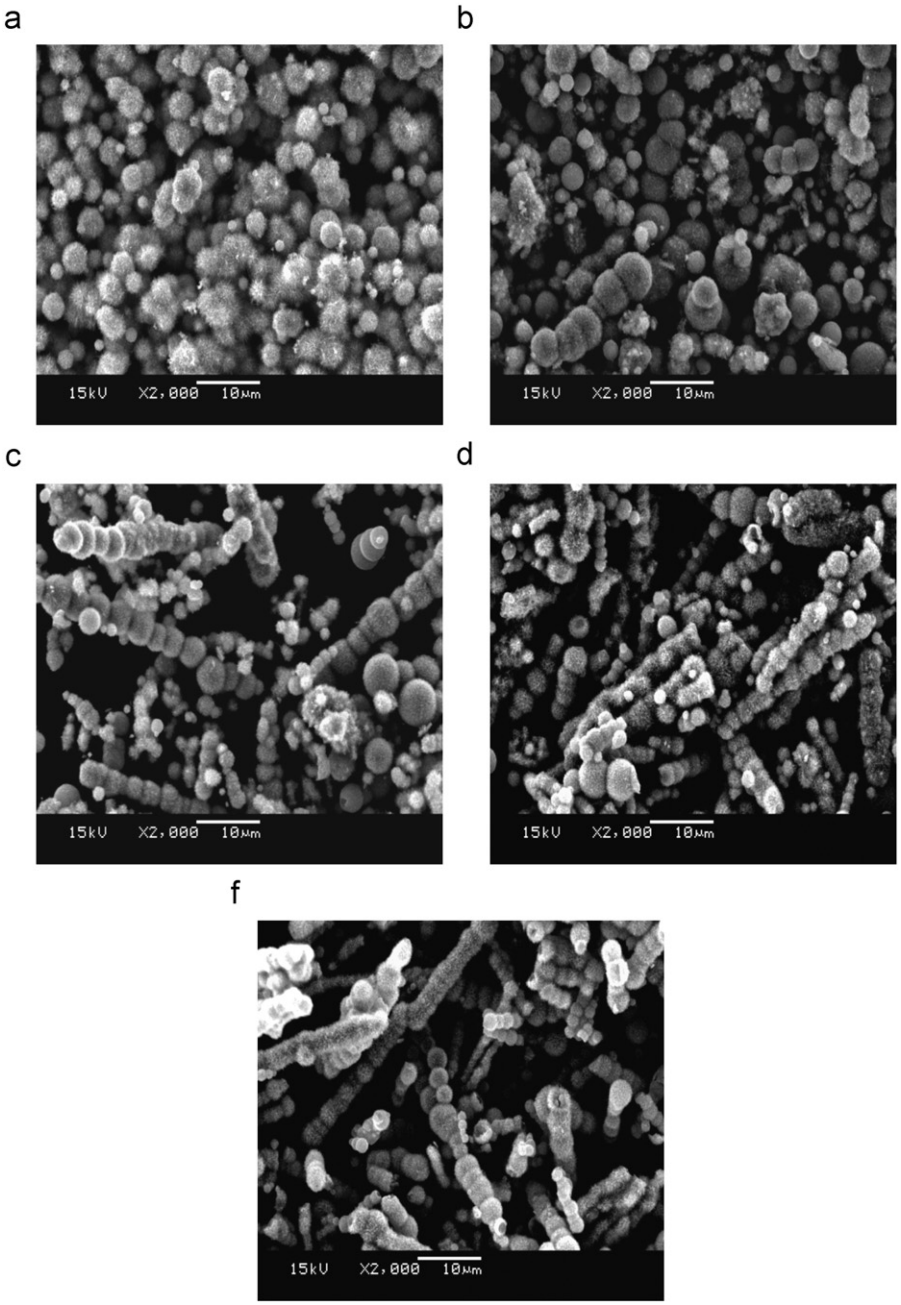

Fig. 1. SEM images of the MnO_2 samples synthesized at 70 °C for 4 h. (a) Without a high magnetic field, (b) with a magnetic field strength of 1 T, (c) with a magnetic field strength of 3 T, (d) with a magnetic field strength of 5 T, and (e) with a magnetic field strength of 8 T.

$\mu'' \approx 0.017$. When the external magnetic field strength was 3 T, the values of μ' and μ'' appeared as a large peak at 5.76 GHz, which is expected when magnetic loss has been improved.

Fig. 5 shows the frequency dependence of the electric loss tangent and magnetic loss tangent of the five samples. In Fig. 5 (a), the electric loss tangent values of the five samples are fluctuant with increasing frequency in the 2–18 GHz range. Magnetic field strength increased, the electric loss tangent values for the five samples decreased, except for 1 T. The electric loss tangent values of the five samples were 0.37–0.42, 0.39–0.43, 0.29–0.33, 0.20–0.24, and 0.20–0.23. As shown in Fig. 5 (b), the magnetic loss tangent values of 0 and 1 T were almost constant, with less variation throughout the whole frequency range. However, the magnetic loss tangent values of 3, 5, and 8 T had clearly increased compared with those of 0 and 1 T. As 3 T, the magnetic loss tangent value reached an expected improvement in the whole frequency and a maximum peak at 5.76 GHz, which corresponded to the data depicted in Fig. 4 (b). However, with further sequential increases in magnetic field strength, the magnetic loss tangent values gradually decreased. The magnetic loss tangent values of the five samples were 0.001–0.025, 0.002–0.035, 0.029–0.420, 0.020–0.126, and 0.001–0.047. Therefore, the electromagnetic loss property of the 3 T sample was more favorable among the five samples. The possible reasons are as follows:

The attenuation of electromagnetic wave in the x department $I_{(x)}$ is given by [25]

$$I_{(x)} = I_0 \exp(-n\sigma_{ex}x) \quad (1)$$

where $I_{(0)}$ is the incident energy of electromagnetic waves, n the number of absorbent particles per unit volume, and σ_{ex} the

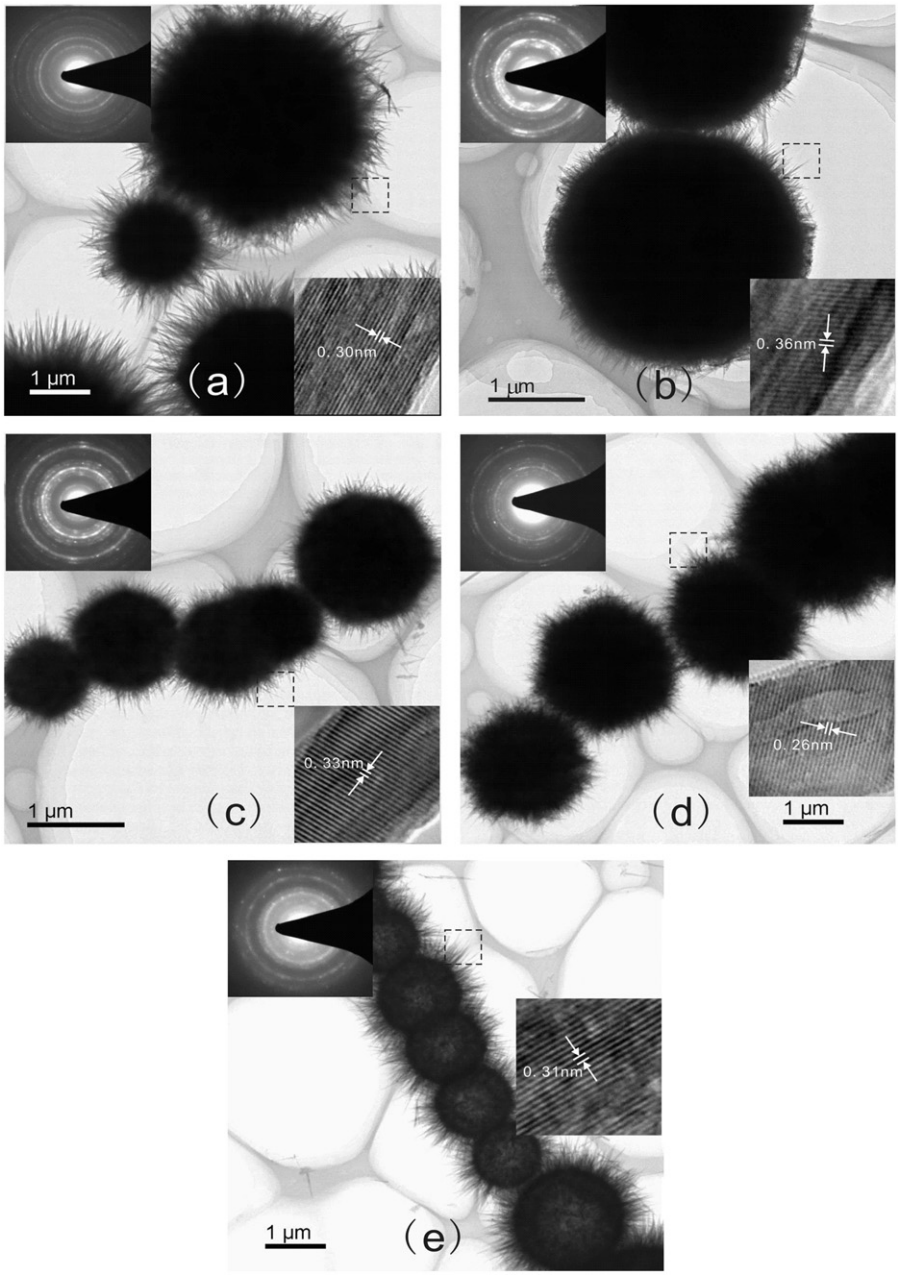

Fig. 2. TEM images with inserted diffraction patterns and the HRTEM images of the MnO_2 samples synthesized at 70 °C for 4 h. (a) Without a high magnetic field, (b) with a magnetic field strength of 1 T, (c) with a magnetic field strength of 3 T, (d) with a magnetic field strength of 5 T, and (e) with a magnetic field strength of 8 T. The HRTEM images were obtained from the stick on the surface of the MnO_2 micro-sphere, which were marked with the rectangular regions.

extinction cross section of the particles. According to Eq. (1), for a larger n, a larger extinction cross section σ_{ex} is obtained, so there is a greater electromagnetic wave attenuation of the particles. Due to the smaller particle size of the 3 T sample, compared to the other samples, the extinction cross section σ_{ex} is larger, which will aid in the improvement of the magnetic loss. Furthermore, according to the phase structure and composition in Fig. 3, the crystalline nature and percentage of α- and γ-phase MnO_2 in each sample will play an important role for their electromagnetic properties [26].

Based on this analysis, an external high magnetic field can be seen to have substantial effects on the electromagnetic properties of a prepared MnO_2 powder. The dielectric constant and the loss tangent clearly decreased under the magnetic field. The imaginary part of the magnetic permeability and magnetic loss tangent substantially increased, while the real part of the magnetic permeability, except for 3 T, was almost constant, with less variation, compared to MnO_2 prepared in the absence of an external magnetic field.

3.4. Electromagnetic wave absorption properties

To further confirm the dependence of the microwave absorption properties on the permittivity and the permeability, the reflection losses [R(dB)] were calculated according to the transmission line theory [27]. The normalized input impedance Z_{in} of a microwave absorber is given by

$$Z_{in} = \sqrt{\frac{\mu_r}{\varepsilon_r}} \tanh\left[j\frac{2\pi}{c}\sqrt{\mu_r}\varepsilon_r fd \right] \quad (2)$$

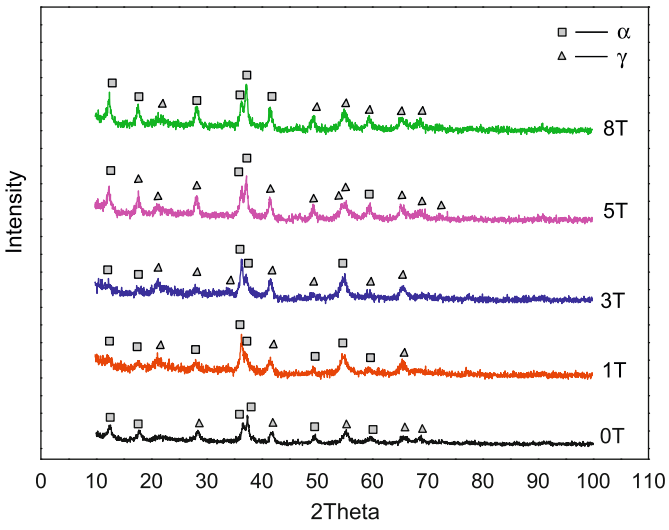

Fig. 3. XRD patterns of the as-synthesized samples with 0, 1, 3, 5, and 8 T.

where μ_r and ε_r are the relative permeability and permittivity of the composite medium, c the velocity of electromagnetic waves in free space, f the frequency of the microwave, and d the thickness of the absorber. The reflection loss is related to Z_{in} as

$$\text{Reflection loss (dB)} = 20\log\left|\frac{Z_{in}-Z_0}{Z_{in}+Z_0}\right| \quad (3)$$

where $Z_0 = \sqrt{\mu_0/\varepsilon_0}$ is the characteristic impedance of free space.

Fig. 6 shows the theoretically calculated values of reflection loss versus frequency according to Eqs. (2) and (3). Clearly, when the magnetic field strength increases, except for 1 T, the absorption peaks become smoother and shift to a higher frequency. Over the whole range from 2 to 18 GHz, the reflection loss values of 0, 1 and 8 T only had one absorption peak. However, the reflection loss values for 3 and 5 T have two absorption peaks, which attributes mainly to the resonance peak frequency of the corresponding complex relative permeability (see Fig. 4) and wave interference on the fore and after surface of the sample. In the frequency range 2–18 GHz, the 0 and 1 T

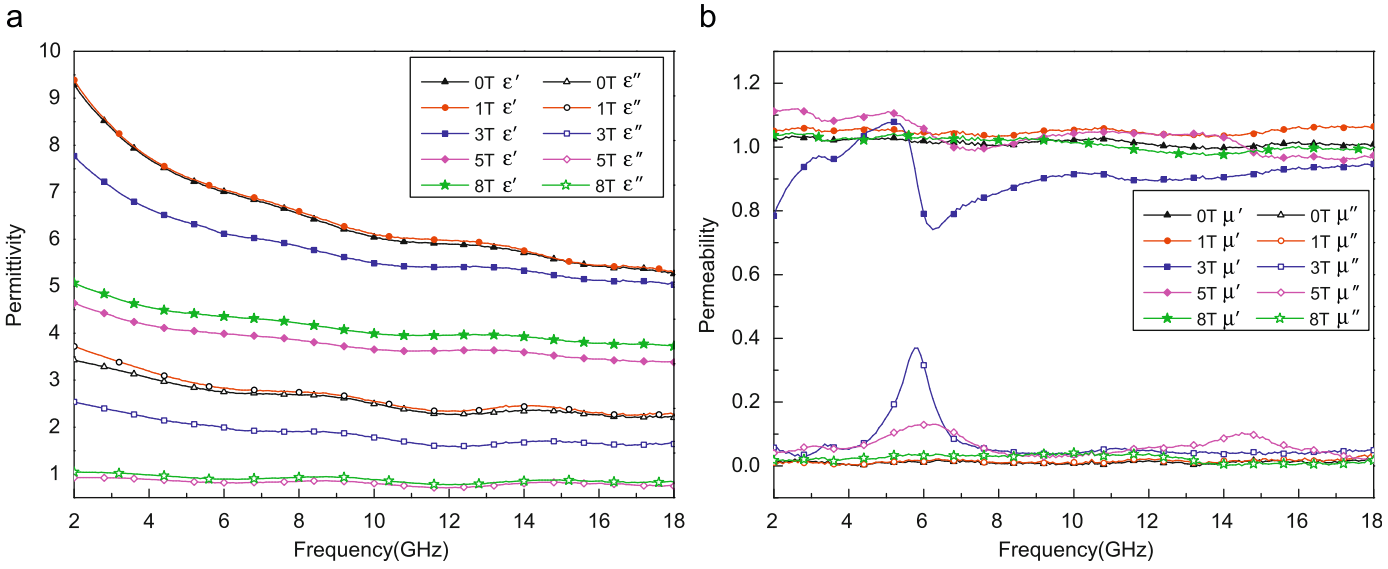

Fig. 4. The relative complex permittivity and permeability of the five samples.

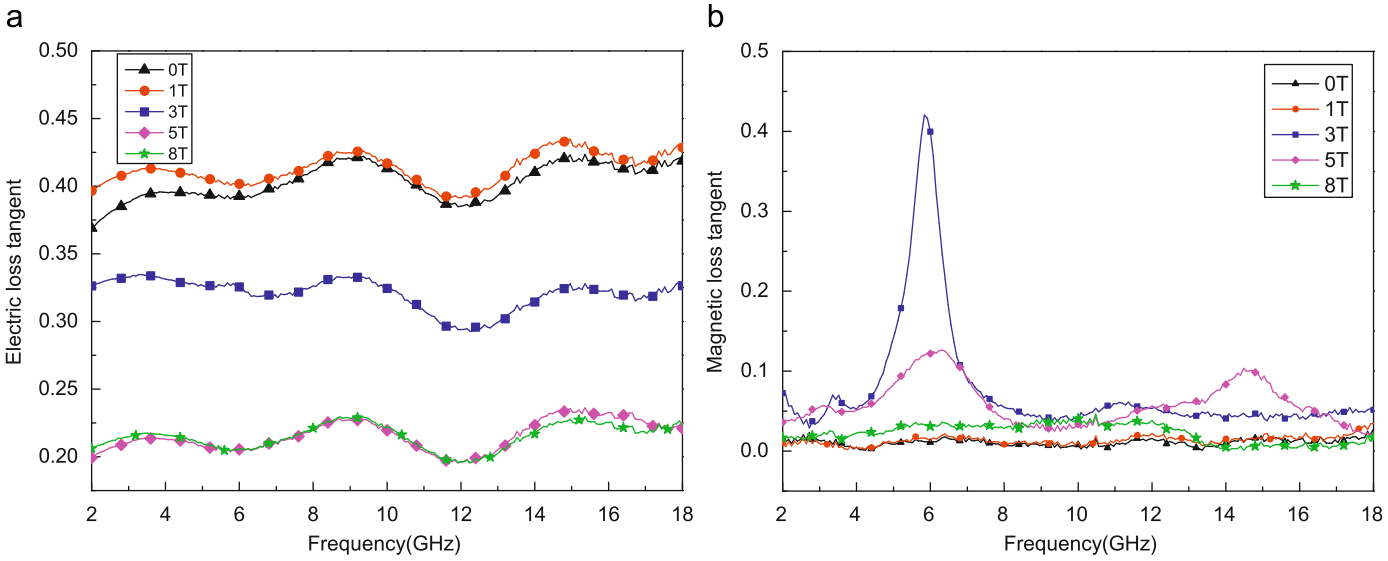

Fig. 5. The electric loss tangent and magnetic loss tangent of the five samples.

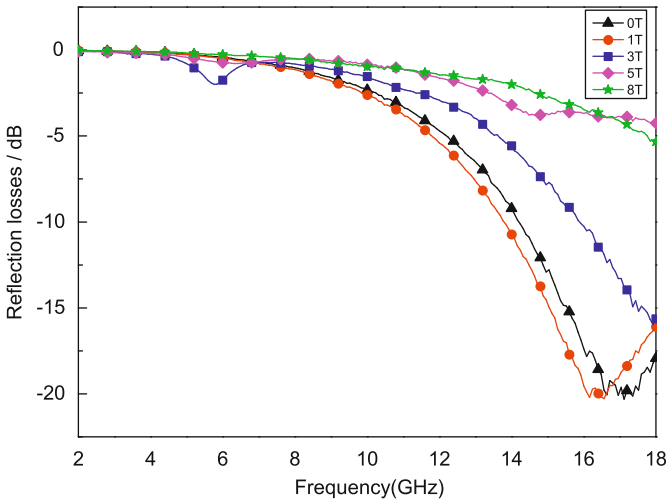

Fig. 6. Reflection loss of the 30 wt% MnO_2/paraffin wax composites with a 2 mm thickness versus frequency (2–18 GHz).

samples show the maximum reflection loss of about −20.3 dB at 17.12 and 16.56 GHz, and the effective absorption band below −10 dB are from 14.24 to 18 GHz and 13.84 to 18 GHz, respectively. The more real parts of the complex permittivity, the higher frequency, the more is wave reflection on the samples. So the absorbing peaks shift to lower frequency band with increasing real parts of the complex permittivity. Furthermore, the dielectric polarization loss versus frequency of MnO_2 with different crystalline structure also plays an important role on the shifts of the absorption peaks.

4. Conclusions

MnO_2 materials with a sea urchin-like ball chain shape were successfully obtained by the synthesis in a high magnetic field. The major components were α-MnO_2 and γ-MnO_2. The electromagnetic properties revealed a clearly decreased dielectric constant and loss tangent for materials synthesized under a magnetic field. The imaginary part of the magnetic permeability and magnetic loss tangent increased remarkably. In addition, the absorption peaks, except for the 1 T sample, become smoother and shifted to a higher frequency. The 0 and 1 T samples showed maximum reflection loss in the frequency range 2–18 GHz.

Acknowledgments

The authors acknowledge the support from The Research Fund for the Doctoral Program of Higher Education of China (No.20090041120038), The Aero Science Foundation of China (20095463008), The Research Fund for the Advanced Research of the Weapon Equipment of China (No: 2009317), The National R&D Infrastructure and Facility Development Program of China (2005DKA10400) and the Growth Foundation for the Youth Teachers of the Dalian University of Technology.

Appendix A. Supplementary data

Supplementary data associated with this article can be found in the online version at doi:10.1016/j.jssc.2010.04.027

References

[1] G. Xi, Y. Peng, Y. Zhu, L. Xu, W. Zhang, W. Yu, Y. Qian, Materials Research Bulletin 39 (2004) 1641–1648.
[2] L. Li, Y. Chu, Y. Liu, L. Dong, Materials Letters 61 (2007) 1609–1613.
[3] X.F. Zhang, X.L. Dong, H. Huang, Y.Y. Liu, W.N. Wang, X.G. Zhu, B. Lv, J.P. Lei, Applied Physics Letters 89 (2006) 053115.
[4] J.H. Du, C. Sun, S. Bai, G. Su, Z. Ying, H.M. Cheng, Journal of Materials Research 17 (5) (2002) 1232–1236.
[5] Y.P. Duan, S.H. Liu, H.T. Guan, Journal of Composite Materials 40 (12) (2006) 1093–1104.
[6] H.M. Huang, S. Mao, H. Feick, H. Yan, Y. Wu, H. King, E. Weber, R. Russo, P. Yang, Science 292 (2001) 1897–1899.
[7] A.R. Armstrong, P.G. Bruce, Nature 381 (1996) 499–500.
[8] B. Ammundsen, J. Paulsen, Advance Materials 13 (2001) 943–956.
[9] F. Xu, T. Wang, W.R. Li, Z.Y. Jiang, Chemical Physics Letters 375 (2003) 247.
[10] S. Bach, M. Henry, N. Baer, J. Livage, Journal of Solid State Chemistry 88 (1990) 325.
[11] X.M. Liu, S.Y. Fu, C.J. Huang, Powder Technology 154 (2005) 120–124.
[12] Y. Chen, C. Liu, F. Li, H.M. Cheng, Journal of Alloys and Compounds 397 (2005) 282–285.
[13] Y. Liu, M. Zhang, J. Zhang, Y. Qian, Journal of Solid State Chemistry 179 (2006) 1757–1761.
[14] X. Sun, C. Ma, Y. Wang, H. Li, Inorganic Chemistry Communications 5 (2002) 747–750.
[15] Y. Zheng, Y. Cheng, F. Bao, Y. Wang, Y. Qin, Journal of Crystal Growth 286 (2006) 156–161.
[16] H.E. Wang, D. Qian, Materials Chemistry and Physics 109 (2008) 399–403.
[17] H. Luo, M. Wei, K. Wei, Journal of Crystal Growth 310 (2008) 2738–2741.
[18] E. Beaudrouet, A. Salle, D. Guyomard, Electrochimica Acta 54 (2009) 1240–1248.
[19] M. Liu, G. Zhang, Z. Shen, P. Sun, D. Ding, T. Chen, Solid State Sciences 11 (2009) 118–128.
[20] F.Y. Cheng, J.Z. Zhao, W.E. Song, C.S. Li, H. Ma, J. Chen, P.W. Shen, Inorganic Chemistry 45 (2006) 2038–2044.
[21] Y.G. Zhang, L.Y. Chen, Z. Zheng, F.L. Yang, Solid State Sciences 11 (7) (2009) 1265–1269.
[22] C. Zhong, J.Z. Wang, Z.Z. Zhu, S.L. Chou, Z.X. Chen, Y. Li, H.K. Liu, Hydrothermal synthesis of nanostructured MnO_2 under magnetic field for rechargeable lithium batteries, Journal of Solid State Electrochemistry, doi: 10.1007/s10008-009-0992-1 (online available in December).
[23] C.H. Gong, L.G. Yu, Y.P. Duan, J.T. Tian, Z.S. Wu, Z.J. Zhang, European Journal of Inorganic Chemistry (18) (2008) 2884–2891.
[24] N. Chen, G.H. Mu, X.F. Pan, K.K. Gan, M.Y. Gu, Materials Science and Engineering 139 (2007) 256–260.
[25] F.D. Ge, J. Zhu, L.M. Chen, Acta Electronica Sinica 24 (1996) 82–86.
[26] Y. Duan, H. Ma, X. Li, S. Liu, Z. Ji, Physica B: Condensed Matter 405 (7) (2010) 1826–1831.
[27] Y. Natio, K. Suetake, IEEE Transactions on Microwave Theory and Techniques 19 (1) (1971) 65–72.